

PHOTOMETRY OF 10 MILLION STARS FROM THE FIRST TWO YEARS OF TESS FULL FRAME IMAGES

Chelsea X. Huang,^{1,*} Andrew Vanderburg,² Andras Pál,¹ Lizhou Sha,^{1,2} Liang Yu,¹ Willie Fong,¹ Michael Fausnaugh,¹ Avi Shporer,¹ Natalia Guerrero,¹ Roland Vanderspek,¹ and George Ricker¹

¹*Kavli Institute for Astrophysics and Space Research, Massachusetts Institute of Technology, Cambridge, MA, USA 02139*

²*Department of Astronomy, University of Wisconsin-Madison*

(Revised November 13, 2020)

ABSTRACT

The Transiting Exoplanet Survey Satellite (TESS) is the first high-precision full-sky photometry survey in space. We present light curves from a magnitude limited set of stars and other stationary luminous objects from the TESS Full Frame Images, as reduced by the MIT Quick Look Pipeline (QLP). Our light curves cover the full two-year TESS Primary Mission and include $\sim 14,770,000$ and $\sim 9,600,000$ individual light curve segments in the Southern and Northern ecliptic hemispheres, respectively. We describe the photometry and detrending techniques we used to create the light curves, and compare the noise properties with theoretical expectations. All of the QLP light curves are available at MAST as a High Level Science Product via [10.17909/t9-r086-e880^{a\)}](https://archive.stsci.edu/t9-r086-e880). This is the largest collection of TESS photometry available to the public to date.

Keywords: TESS — survey — pipeline

INTRODUCTION

NASA’s Transiting Exoplanet Survey Satellite (TESS) mission launched on 2018 April 18, and began science operations on 2018 July 25. TESS uses four identical cameras to observe stars over a total $24^\circ \times 96^\circ$ field of view. Like its predecessor, *Kepler*, TESS observes stars in so-called “postage stamps,” or small subimages from the TESS cameras centered on particularly bright or important stars. Unlike *Kepler*, however, TESS also saves and downloads images from its entire field of view every 30 minutes. These full frame images (or FFIs) greatly increase the mission’s discovery space (with some simulations projecting tens of thousands of planet discoveries from the FFIs (Barclay et al. 2018; Huang et al. 2018a), but also substantially increase data processing requirements.

Before TESS’s launch, sophisticated and highly successful software tools were developed to analyze data from space missions like CoRoT (Auvergne et al. 2009) and Kepler (Jenkins et al. 2010). However, because none of these missions downloaded continuous FFIs, the architectures of these pipelines are difficult to adapt to a mission like TESS. In the meantime, unhindered by data downlink rates, ground-based transit surveys like HAT (Bakos et al. 2007, 2013), WASP (Pollacco et al. 2006), and KELT (Pepper et al. 2007, 2012) have been extracting light curves and searching for planets from full frame data for many years. These pipelines (e.g. Collier Cameron et al. 2009; Pál 2009, , etc.) are well suited for analyzing large volumes of wide field images.

Here, we present light curves for a magnitude limited sample of stars observed by TESS produced by the MIT Quick Look Pipeline (QLP). The QLP, whose architecture includes heritage from both ground-based photometric surveys and methods developed for analysis of space-based photometry, was built to rapidly process TESS data as soon as it is beamed to Earth. The QLP has already been used to identify and alert planet candidates throughout the entire TESS Primary Mission, leading to the discovery of more than 1000 planetary candidates (Guerrero et al. 2020, *submitted to ApJS*), dozens of which have already been confirmed (e.g. Huang et al. 2018b; Vanderspek et al. 2019; Huang et al.

Corresponding author: Chelsea X. Huang
xuhuang@mit.edu

^{a)} <https://archive.stsci.edu/hlsp/qlp>

* Torres Postdoctoral Fellow

2020; Armstrong et al. 2020). Here, we describe how QLP produces light curves and evaluate its performance in terms of photometric precision. We publicly release QLP light curves for all sources in the TESS Input Catalog (TIC, Stassun et al. 2018, 2019) observed by TESS in its primary mission down to a limiting TESS magnitude T of 13.5.

LIGHT CURVE EXTRACTION

We extract light curves for all stars in the TIC with TESS magnitude brighter than 13.5 observed in the TESS Primary mission (UT 2018 July 25 - UT 2020 July 04). Figure 1 shows the sky locations of stars with QLP light curves. We also added in stars with proper motion larger than 200 mas yr^{-1} and brightness between TESS Magnitude 13.5 and 15.

Our procedure is as follows:

1. We process the TESS FFIs using the TICA software, which will be described by Fausnaugh et al. (in prep.). The TICA software carries out correction of various instrumental effects described in Vanderspek et al. (2019).
2. The images then go through a global background subtraction using nebuliser (Irwin 1985). Because TESS orbits the Earth, its cameras experience significant levels of scattered background light. Nebuliser removes much of the large-scale scattered background features in the images (features with spatial variation scale >20 pixels).
3. We then determine an astrometric solution for each image following Huang et al. (2015) by relating the measured centroids of bright sources ($8 < T < 10$) to their coordinates in the TIC. This astrometric solution is then used to obtain the precise position of all catalog sources in the images. The typical astrometric precision for each frame is better than 0.1 pixel ($2''.1$).
4. A reference image is constructed with the median combination of 40 good quality images (images with minimal scattered light, as well as good pointing stability), which we identify within each TESS orbit. We then compute difference images for each frame by directly subtracting the reference frame from each individual frames.
5. We measure the differential source brightness from the difference images by summing the flux within a series of 5 circular apertures with different radii (1.75, 2.5, 3.0, 3.5 and 8.0 pixels) centered on these positions. We continue to process the light curves from all five different apertures identically.
6. We then perform a second step of background subtraction. Nebuliser effectively removes large background variations, but leaves in some small-scale features. We therefore estimate the background light levels in the difference images at the position of each source by calculating the median pixel values (with iterative outlier rejection) within annuli around the target stars. The background annuli have inner radius and width of 4.0/3.0, 4.0/3.0, 4.0/3.0, 5.0/4.0 and 10.0/5.0 pixels, respectively. We subtract this background estimate from the difference fluxes for each source.
7. Finally, we convert the measured difference fluxes into absolute fluxes by adding the expected flux from each source based on the TESS-band magnitude estimates from the TIC and the instrument zeropoint magnitude (Vanderspek et al. 2018). This is equivalent to deblending the flux time series assuming the variations observed are from the target star.
8. The time series for each light curve is corrected to the Solar System barycentric reference frame from the TESS spacecraft reference frame following the procedure described by Eastman et al. (2010) Sector 2.1 using the coordinates of the target star at Epoch J2000, and TESS orbits vectors from JPL horizon ¹.

The time series extracted from this step is called the “raw light curve” and are post-processed to prepare for the needs of transit search.

LIGHT CURVE POST-PROCESSING

TESS light curves usually contain low-frequency variability from stellar activity or instrumental noise, which must be filtered before the small, short-duration signals caused by transiting planets can be readily detected. We therefore

¹ <https://ssd.jpl.nasa.gov/horizons.cgi>

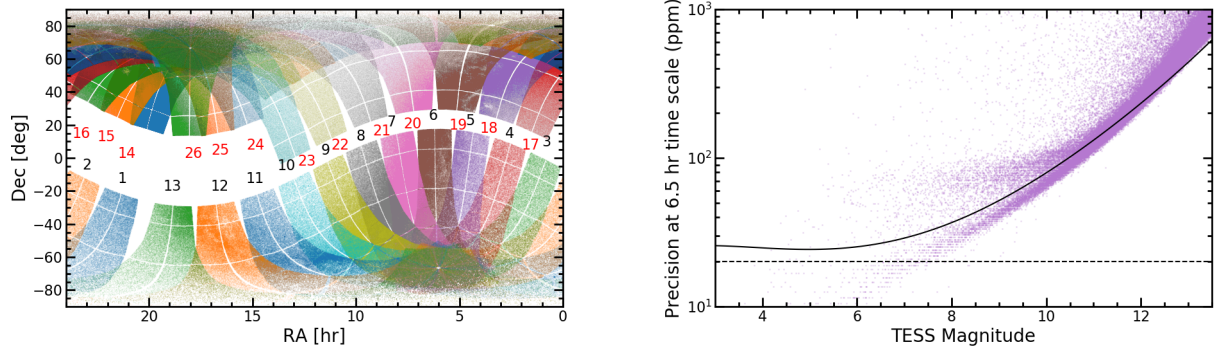


Figure 1. Left: An illustration of all the stars for which we extracted photometry from the TESS Primary Mission FFIs in terms of their equatorial coordinates. Right: The photometric precision of the time series, compared to expected theoretical precision estimated in [Sullivan et al. \(2015\)](#) (solid line). The dashed horizontal line is a reference indicating 20 ppm precision.

detrend the light curves by applying a high-pass filter before they are searched for transits. Before detrending, we reject outliers in the light curve using the quaternion time series². Any exposure corresponding to abnormal amplitudes of scatter in the quaternion time series are not used in the detrending. We then fit the light curves from each spacecraft orbit with a basis spline ([Vanderburg & Johnson 2014](#)). We choose the spacing of the spline break points by minimizing the Bayesian Information Criterion following [Shallue & Vanderburg \(2018\)](#), imposing a minimum allowed spacing of 0.3 days. This minimum spacing is optimized for the detection of planets with short orbital periods; more aggressive splines would lead to the distortion of long-duration transits.

After detrending, we identify anomalous exposures where light curves tend to be noisier than expected based on TESS’s typical photometric precision. For each exposure, we look at the set of stars with TESS magnitude between 9.5 and 10 and calculate the fraction which exhibit photometric precision more than 75% worse than the pre-flight anticipated photometric precision of 200 parts per million (ppm) per hour for stars with $T = 10$ mag. If more than 20 % of the stars observed on the same CCD have poor precision at a particular exposure, we assign a bad quality flag to the corresponding exposure. This bad quality flag is stored as bit 13 in the QUALITY column provided in the light curve products. The rest of the bits are adopted from the SPOC Full Frame Image headers ([Jenkins 2015](#); [Jenkins et al. 2016](#)).

We combine the detrended light curves observed in two TESS orbits of each TESS sector by offsetting the median of the light curves to the expected TESS magnitude, after rejecting bad quality points. These magnitude time series are then converted to normalized flux time series in the final light curve products.

The QLP produces light curves of each source from up to five apertures. We identify an optimal light curve for each target based on the source’s brightness. Early in the mission, we calculated the photometric precision in each aperture for a set of stars and determined the aperture size that yielded the best photometric precision as a function of TESS-band magnitude (in 13 evenly spaced bins between TESS mag of 6 to 13.5). We used these results to select the optimal aperture. We provide “raw light curve” from the optimal aperture in the FITS file of QLP HLSP product on MAST under keywords **SAP_FLUX**. We provided flattened light curves from three apertures with different sizes. The light curve from the optimal aperture is under FITS keyword **KSPSAP_FLUX**. The light curve from the relatively bigger/smaller apertures are under FITS keyword **KSPSAP_FLUX_LAG** and **KSPSAP_FLUX_SML**, respectively.

We show the precision of our light curves in Figure 1. For comparison, the solid line is the theoretical photometric precision estimated by [Sullivan et al. \(2015\)](#) scaled to a 6.5 hr time scale assuming Gaussian noise. The photometric precision roughly follows the predictions for the majority of the stars and has a lower noise floor (approximately 20 ppm) for the brightest stars when the spacecraft operates nominally³.

CAVEATS

² The quaternion series can be downloaded from <https://archive.stsci.edu/missions/tess/engineering/>. For more details see ([Vanderburg et al. 2019](#))

³ The in-orbit performance of the TESS photometers is better than preflight calculations by [Sullivan et al. \(2015\)](#), which has been traced to an underestimation in their assumed telescope aperture.

QLP light curve production depends critically on the *TESS* band magnitudes estimated by the TIC. If a star’s *TESS* band magnitude is incorrect, the amplitude of features in the QLP light curve will be likewise incorrect because the QLP will deblend the light curve incorrectly. The uncertainties of the amplitude of variations in the flux time series therefore depend on the uncertainties in the *TESS* magnitudes. This is not represented in the error-bars we provide in the light curve time series. Instead, the uncertainties are estimated with the Median Absolute Median Deviation statistics of each orbit of light curves multiplied by 1.4826.

We note that light curves from Sectors 1–13 were produced using the TIC version 7, while light curves in Sector 14 onward were produced using TIC version 8. A small fraction of stars have different estimated *TESS* magnitudes in TIC 7 versus TIC 8. These changes in magnitude affect the amount of deblending applied by QLP and thus the amplitude of light curve features.

Our method of deblending the light curve time series also do not take into account that the target stars’ point spread functions may be not fully contained in the smallest circular aperture (with a radius of 1.75 pixel), leading to underestimation of signal amplitudes in this particular aperture for a large fraction of stars.

The TICA software we used to calibrate the *TESS* raw FFIs went through many iterations and version changes during the *TESS* Primary Mission. We did not keep a record of the particular versions of the calibration software used for each sector of data. We expect this issue to be resolved with future data reprocessing and releases. Errors in the TICA smear correction estimate affect the light curves of a small number of stars for one specific version of TICA, so the smear correction was disabled for QLP processing in later sectors. Users can examine light curves of stars located in the same column to identify such contamination.

We thank the entire *TESS* Mission team for years of effort to make this work possible. This paper includes data collected by the *TESS* mission, which are publicly available from the Mikulski Archive for Space Telescopes (MAST). Funding for the *TESS* mission is provided by NASA’s Science Mission directorate. CXH acknowledges support from MIT’s Kavli Institute as a Torres postdoctoral fellow.

Software: *nebuliser* (Irwin 1985), *FITSH* (Pál 2012), *Golang* (Meyerson 2014), *Numpy* (Oliphant 2006–), *Scipy* (Virtanen et al. 2020), *Astropy* (Astropy Collaboration et al. 2013; Price-Whelan et al. 2018)

Facility: *TESS*

REFERENCES

- Armstrong, D. J., Lopez, T. A., Adibekyan, V., et al. 2020, *Nature*, 583, 39, doi: [10.1038/s41586-020-2421-7](https://doi.org/10.1038/s41586-020-2421-7)
- Astropy Collaboration, Robitaille, T. P., Tollerud, E. J., et al. 2013, *A&A*, 558, A33, doi: [10.1051/0004-6361/201322068](https://doi.org/10.1051/0004-6361/201322068)
- Auvergne, M., Bodin, P., Boisdard, L., et al. 2009, *A&A*, 506, 411, doi: [10.1051/0004-6361/200810860](https://doi.org/10.1051/0004-6361/200810860)
- Bakos, G. Á., Noyes, R. W., Kovács, G., et al. 2007, *ApJ*, 656, 552, doi: [10.1086/509874](https://doi.org/10.1086/509874)
- Bakos, G. Á., Csabry, Z., Penev, K., et al. 2013, *PASP*, 125, 154, doi: [10.1086/669529](https://doi.org/10.1086/669529)
- Barclay, T., Pepper, J., & Quintana, E. V. 2018, *ApJS*, 239, 2, doi: [10.3847/1538-4365/aac3e9](https://doi.org/10.3847/1538-4365/aac3e9)
- Collier Cameron, A., Pollacco, D., Hellier, C., et al. 2009, in *IAU Symposium*, Vol. 253, *Transiting Planets*, ed. F. Pont, D. Sasselov, & M. J. Holman, 29–35
- Eastman, J., Siverd, R., & Gaudi, B. S. 2010, *PASP*, 122, 935, doi: [10.1086/655938](https://doi.org/10.1086/655938)
- Huang, C. X., Penev, K., Hartman, J. D., et al. 2015, *MNRAS*, 454, 4159, doi: [10.1093/mnras/stv2257](https://doi.org/10.1093/mnras/stv2257)
- Huang, C. X., Shporer, A., Dragomir, D., et al. 2018a, *arXiv e-prints*, arXiv:1807.11129, <https://arxiv.org/abs/1807.11129>
- Huang, C. X., Burt, J., Vanderburg, A., et al. 2018b, *ApJ*, 868, L39, doi: [10.3847/2041-8213/aaef91](https://doi.org/10.3847/2041-8213/aaef91)
- Huang, C. X., Quinn, S. N., Vanderburg, A., et al. 2020, *ApJL*, 892, L7, doi: [10.3847/2041-8213/ab7302](https://doi.org/10.3847/2041-8213/ab7302)
- Irwin, M. J. 1985, *MNRAS*, 214, 575, doi: [10.1093/mnras/214.4.575](https://doi.org/10.1093/mnras/214.4.575)
- Jenkins, J. M. 2015, in *AAS/Division for Extreme Solar Systems Abstracts*, Vol. 3, *AAS/Division for Extreme Solar Systems Abstracts*, 106.05
- Jenkins, J. M., Caldwell, D. A., Chandrasekaran, H., et al. 2010, *ApJL*, 713, L87, doi: [10.1088/2041-8205/713/2/L87](https://doi.org/10.1088/2041-8205/713/2/L87)
- Jenkins, J. M., Twicken, J. D., McCauliff, S., et al. 2016, *Society of Photo-Optical Instrumentation Engineers (SPIE) Conference Series*, Vol. 9913, *The TESS science processing operations center*, 99133E
- Meyerson, J. 2014, *IEEE software*, 31, 104
- Oliphant, T. 2006–, *NumPy: A guide to NumPy*, USA: Trelgol Publishing. <http://www.numpy.org/>
- Pál, A. 2009, PhD thesis, Department of Astronomy, Eötvös Loránd University
- . 2012, *MNRAS*, 421, 1825, doi: [10.1111/j.1365-2966.2011.19813.x](https://doi.org/10.1111/j.1365-2966.2011.19813.x)
- Pepper, J., Kuhn, R. B., Siverd, R., James, D., & Stassun, K. 2012, *PASP*, 124, 230, doi: [10.1086/665044](https://doi.org/10.1086/665044)
- Pepper, J., Pogge, R. W., DePoy, D. L., et al. 2007, *PASP*, 119, 923, doi: [10.1086/521836](https://doi.org/10.1086/521836)
- Pollacco, D. L., Skillen, I., Collier Cameron, A., et al. 2006, *PASP*, 118, 1407, doi: [10.1086/508556](https://doi.org/10.1086/508556)
- Price-Whelan, A. M., Sipőcz, B. M., Günther, H. M., et al. 2018, *AJ*, 156, 123, doi: [10.3847/1538-3881/aabc4f](https://doi.org/10.3847/1538-3881/aabc4f)
- Shallue, C. J., & Vanderburg, A. 2018, *AJ*, 155, 94, doi: [10.3847/1538-3881/aa9e09](https://doi.org/10.3847/1538-3881/aa9e09)
- Stassun, K. G., Oelkers, R. J., Pepper, J., et al. 2018, *AJ*, 156, 102, doi: [10.3847/1538-3881/aad050](https://doi.org/10.3847/1538-3881/aad050)
- Stassun, K. G., Oelkers, R. J., Paegert, M., et al. 2019, *AJ*, 158, 138, doi: [10.3847/1538-3881/ab3467](https://doi.org/10.3847/1538-3881/ab3467)
- Sullivan, P. W., Winn, J. N., Berta-Thompson, Z. K., et al. 2015, *ApJ*, 809, 77, doi: [10.1088/0004-637X/809/1/77](https://doi.org/10.1088/0004-637X/809/1/77)
- Vanderburg, A., & Johnson, J. A. 2014, *PASP*, 126, 948, doi: [10.1086/678764](https://doi.org/10.1086/678764)
- Vanderburg, A., Huang, C. X., Rodriguez, J. E., et al. 2019, *ApJL*, 881, L19, doi: [10.3847/2041-8213/ab322d](https://doi.org/10.3847/2041-8213/ab322d)
- Vanderspek, R., Doty, J. P., Fausnaugh, M., et al. 2018, *TESS Instrument Handbook*, TESS Science Office
- Vanderspek, R., Huang, C. X., Vanderburg, A., et al. 2019, *ApJL*, 871, L24, doi: [10.3847/2041-8213/aafb7a](https://doi.org/10.3847/2041-8213/aafb7a)
- Virtanen, P., Gommers, R., Oliphant, T. E., et al. 2020, *Nature Methods*, 17, 261, doi: <https://doi.org/10.1038/s41592-019-0686-2>

QLP Data Production Description Documents

This document is a supplement material to the RNAAS article.

1. Introduction

This document describes the primary mission light curve time series format produced by the MIT Quick Look Pipeline. These light curves are available at MAST as a High Level Science Product via [doi:10.17909/t9-r086-e880](https://archive.stsci.edu/hslp/qlp) (<https://archive.stsci.edu/hslp/qlp>).

We try our best to follow the conventions in the data format established by the TESS data release notes. The details are described as the following.

2. Light Curve Files

2.1. Purpose

The QLP light curve files contain the output of flux time series from the photometric analysis on the TESS Full Frame Images and the subsequent detrending step. A single file contains the light curves for one target for one sector (two TESS orbits). Raw photometry is provided from the best aperture, while detrended photometry time series from three apertures are provided. If a target was observed in more than one sector then multiple files will be created.

2.2. Filename Format

The file names of the QLP light curves follow the naming convention below:

`hslp_qlp_tess_ffi_ssctr-tid_tess_vvnum_llc.fits.gz`

Lettering in italics indicates parameters that will be instantiated for some specific instance of a file, for example timestamps and target identifiers. *tid*, is a 16 digit zero-padded target identifier that refers to an entry in the TESS Input Catalog (TIC). *sctr*, is a 4 digit zero-padded integer indicating the sector in which the data were last observed. *vnum*, is a 2 digit number referring the versions of the light curve.

2.3. Composition

We adopt the convention from the official TESS data products for the composition of the FITS files. The primary header contains information about the target that does not vary with the data

acquisition time, such as its TIC ID, coordinates, and stellar information. We default the stellar parameters to -1 if they are not presented in the corresponding catalog. The primary HDU does not have a data table. The second HDU contains a FITS binary table where each row in the table contains the data at some cadence. The definitions of the columns for this table are summarized in table 1. The header for the second HDU contains keywords that are needed to describe the binary table and properties.

2.3.1. Primary Header

The primary header keywords are described in the following Table:

Header Card	Data Type	Example Value
SIMPLE = T / conforms to FITS standard	L1	const
BITPIX = 8 / array data type	I4	const
NAXIS = 0 / number of array dimensions	I4	const
EXTEND = T	L1	const
NEXTEND = 1 / number of standard extensions	I4	const
EXTNAME = 'PRIMARY' / name of extension	C7	const
ORIGIN = 'MIT/QLP' / institution responsible for creating this file	C7	const
TELESCOP = "TESS" / telescope	C4	const
INSTRUME = "TESS Photometer" / detector type	C15	const
FILTER = "TESS" / filter used for observations	C4	const
OBJECT = / string version of TICID	C20	TIC 55129913
TICID = / unique TESS target identifier	I8	55129913
SECTOR= / last observed sector	I4	8
CAMERA = / camera	I2	2
CCD = / ccd	I2	1

RADESYS ="ICRS" / reference frame of celestial coordinates	C4	const
RA_OBJ = / [deg] right ascension, J2000.0	R4	125.640067
DEC_OBJ = / [deg] declination, J2000.0	R4	-32.6201092
TESSMAG = / [mag] TESS magnitude, TIC v8	R4	12.9946
RADIUS = / [solar radii] stellar radius	R4	60.3377
LOGG = / [cm/s ²] log10 surface gravity	R4	-1
MASS = / [solar mass] log10 stellar mass	R4	-1
TEFF = / [K] effective temperature	R4	4725
MH = /metallicity	R4	-1
EQUINOX = 2000.0 / equinox of celestial coordinate system	R8	const
PMRA = / [mas/yr] RA proper motion	R4	-1.98566
PMDEC = / [mas/yr] Dec proper motion	R4	2.747
TICVER = / TIC Version	I4	8
CALIB = / pipeline used for image calibration	C4	TICA
END		

2.3.2. Light curve binary table extension header

The following table summarizes the light curve binary table columns:

Column Number	TYPE	FORM	UNIT	Description
---------------	------	------	------	-------------

1	TIME	64-bit float	Days	BJD - 2457000 (BTJD)
2	CADENCENO	32-bit integer		timestamp count from start of mission
3	SAP_FLUX	32-bit float		Normalized simple aperture photometry light curve from the best aperture
4	KSPSAP_FLUX	32-bit float		Normalized light curve detrended by kepler spline
5	KSPSAP_FLUX_ERR	32-bit float		1 σ uncertainty of the KSPSAP light curve.
6	QUALITY	32-bit integer	Bit field	Each bit is a flag defined in section 2.3.3.
7	ORBITID	32-bit integer		The orbit number count from start of mission
8	SAP_X	32-bit float	pixels	CCD column position of target's flux-weighted centroid.
9	SAP_Y	32-bit float	pixels	CCD row position of target's flux-weighted centroid.
10	SAP_BKG	32-bit float		Estimated background flux contribution to the target aperture. Already subtracted from SAP_FLUX, and a median image.
11	SAP_BKG_ERR	32-bit float		1 σ uncertainty of

				the SAP background light curve.
12	KSPSAP_FLUX_SML	32-bit float		Detrended normalized simple aperture photometry light curve from a smaller aperture
13	KSPSAP_FLUX_LAG	32-bit float		Detrended normalized simple aperture photometry light curve from a larger aperture

The following table summarizes the keywords in the second HDU.

Header Card	Data Type	Example Value
XTENSION= 'BINTABLE' / binary table extension	C8	const
BITPIX = 8 / array data type	I4	const
NAXIS = 2 / number of array dimensions	I4	const
NAXIS1 = 56 / length of dimension 1	I4	const
NAXIS2 = / length of dimension 2	I4	1200
PCOUNT = 0 / number of group parameters	I4	const
GCOUNT = 1 / number of groups	I4	const
TFIELDS = 13 / number of table fields	I4	const
TTYPE1 = 'TIME ' / column title: data time stamps	C4	const
TFORM1 = 'D ' / column format: 64-bit floating point	C1	const
TUNIT1 = 'BJD - 2457000, days' / column units: Barycenter corrected TESS Julian Date	C15	const
TTYPE2 = 'CADENCENO' / column title: unique cadence number	C9	const

TFORM2 = 'J' / column format: signed 32-bit integer	C1	const
TTYPE3 = 'SAP_FLUX' / column title: normalized aperture photometry flux	C8	const
TFORM3 = 'E' / column format: 32-bit floating point	C1	const
TTYPE4 = 'KSPSAP_FLUX' / column title: detrended aperture photometry flux	C11	const
TFORM4 = 'E' / column format: 32-bit floating point	C1	const
TTYPE5 = 'KSPSAP_FLUX_ERR' / column title: normalized detrended aperture photometry flux err	C15	const
TFORM5 = 'E' / column format: 32-bit floating point	C1	const
TTYPE6 = 'QUALITY' / column title: aperture photometry quality flag	C7	const
TFORM6 = 'J' column format: signed 32-bit integer	C1	const
TTYPE7 = 'ORBITID' / column title: unique orbit number	C7	const
TFORM7 = 'J' column format: signed 32-bit integer	C1	const
TTYPE8 = 'SAP_X' / column title: derived weighted column centroid in aperture	C5	const
TFORM8 = 'E' / column format: 32-bit floating point	C1	const
TUNIT8 = 'pixel' / column units: pixel	C5	const
TTYPE9 = 'SAP_Y' / column title: derived weighted row centroid in aperture	C5	const
TFORM9 = 'E' / column format: 32-bit floating point	C1	const
TUNIT9 = 'pixel' / column units: pixel	C5	const
TTYPE10 = 'SAP_BKG' / column title: aperture phot. background flux	C7	const
TFORM10 = 'E' / column format: 32-bit floating point	C1	const
TTYPE11 = 'SAP_BKG_ERR' / column title: ap. phot. background flux error	C11	const
TFORM11 = 'E' / column format: 32-bit floating point	C1	const
TTYPE12 = 'SAP_FLUX_SML' / column title: normalized small aperture photometry flux	C12	const
TFORM12 = 'E' / column format: 32-bit floating point	C1	const

TTYPE13 = 'SAP_FLUX_LAG' / column title: normalized large aperture photometry flux	C12	const
TFORM13 = 'E' / column format: 32-bit floating point	C1	const
INHERIT = T / inherit the primary header	C1	const
EXTNAME = 'LIGHTCURVE' / name of extension	C10	const
EXTVER = 1 / extension version number (not format version)	I4	const
TELESCOP= 'TESS' / telescope	C4	const
INSTRUME= 'TESS Photometer' / detector type	C15	const
OBJECT = / string version of TICID	C20	TIC 55129913
TICID= / unique TESS target identifier	I8	55129913
RADESYS = 'ICRS' / reference frame of celestial coordinates	C4	const
RA_OBJ = / [deg] right ascension	R4	125.64006 7
DEC_OBJ = / [deg] declination	R4	- 32.620109 2
EQUINOX = 2000.0 / equinox of celestial coordinate system	R8	const
TIMEREFS = 'SOLARSYSTEM' / barycentric correction applied to times	C11	const
TASSIGN = 'SPACECRAFT' / where time is assigned	C10	const
TIMESYS = 'TDB' / time system is Barycentric Dynamical Time (TDB)	C3	const
BJDREFI = 2457000 / integer part of BJD reference date	I4	const
BJDREFF = 0.0 / fraction of the day in BJD reference date	R4	const
TIMEUNIT= 'd' / time unit for TIME, TSTART and TSTOP	C1	const
TELAPSE = / [d] TSTOP - TSTART	R4	27.0
TSTART = / observation start time in TBJD	R4	1630.2
TSTOP = / observation stop time in TBJD	R4	1657.2
TIMEDEL = / [d] time resolution of data	R4	0.02083
MJD-BEG = / observation start time in MJD	R4	58629.5

MJD-END = / observation end time in MJD	R4	58656.5
BESTAP = / [pix] the radius and background aperture of the best aperture	C12	3.0:4.0:3.0
SMALLAP = / [pix] the radius and background aperture of the smaller aperture	C12	2.5:4.0:3.0
LARGEAP = / [pix] the radius and background aperture of the larger aperture	C12	3.5:4.0:3.0
KSPPENCO = / the penalty coefficient used in the detrending	R4	0.75
KSPBSMIN = / [d] the minimum break space used in the detrending	R4	0.75
KSPBSMAX = / [d] the maximum break space used in the detrending	R4	1.5

2.3.3. Quality Flags

The light curve files include an integer table column that describes any anomalies detected in the data for that cadence or image. These integers should be treated as individual bits that have the meanings summarized as below. We adopt the bits definition from the SPOC TESS Full Frame Image data product. We then added one extra bit (bit 13, value 4195) using our own anomaly detection algorithm described in the RNAAS article, Section Lightcurve Post Processing.

Only 9 different bits are used for the quality flags of these full frame image light curves. They are the following:

Bit	Value	Description
1	1	Attitude tweak
3	4	Spacecraft in coarse pointing
4	8	Spacecraft in Earth pointing
5	16	Argabrightening event
6	32	Reaction Wheel desaturation Event
8	128	Manual Exclude.
11	1024	Cosmic ray detected on collateral pixel row or column.
12	2048	Straylight from Earth or Moon in camera FOV.

13	4196	Low precision points. The cadence was excluded because low precision data occurred in a large fraction of the stars
----	------	---

3. Alternative format of light curves

3.1 Purpose

We provide a light weighted format of the QLP light curve files in comma separated ascii files. A single file contains the light curves for one target for one sector (two orbits). Only normalized raw photometry and normalized background flux in the good quality cadences are provided from the best aperture. If a target was observed in more than one sector then multiple files will be created.

3.2. Filename Format

The file names of the QLP light curves follow the naming convention below:

hlsp_qlp_tess_ffi_ssctr-*tid*_tess_vvnum_llc.txt

Lettering in italics indicates parameters that will be instantiated for some specific instance of a file, for example timestamps and target identifiers. *tid*, is a 16 digit zero-padded target identifier that refers to an entry in the TESS Input Catalog (TIC). *sctr*, is a 4 digit zero-padded integer indicating the sector in which the data were last observed. *vnum*, is a 2 digit number referring the versions of the light curve.

3.3. Composition

Column header	Format	Description
Time (BTJD)	R4	[Days] BJD - 2457000 (BTJD)
Normalized SAP_FLUX	R4	Normalized simple aperture photometry flux time series from the best aperture with bad cadences rejected.
Normalized SAP_BKG	R4	Normalized simple aperture background flux time series with bad cadences rejected. The scatter of the background flux time series is scaled to be

		similar to that of the flux time series.
--	--	--